ACS central science

Research Article

http://pubs.acs.org/journal/acscii

A Multichannel Biosensor for Rapid Determination of Cell Surface Glycomic Signatures

Subinoy Rana,[†,‡] Ngoc D. B. Le,[†,§] Rubul Mout,[†,§] Bradley Duncan,[†,§] S. Gokhan Elci,[†] Krishnendu Saha,[†] and Vincent M. Rotello*[,†]

[†]Department of Chemistry, University of Massachusetts Amherst, 710 North Pleasant Street, Amherst, Massachusetts 01003, United States

[‡]Department of Materials, Imperial College London, London SW7 2AZ, United Kingdom

Supporting Information

ABSTRACT: Cell surface glycosylation serves a fundamental role in dictating cell and tissue behavior. Cell surface glycomes differ significantly, presenting viable biomarkers for identifying cell types and their states. Glycoprofiling is a challenging task, however, due to the complexity of the constituent glycans. We report here a rapid and effective sensor for surface-based cell differentiation that uses a three-channel sensor produced by noncovalent conjugation of a functionalized gold nanoparticle (AuNP) and fluorescent proteins. Wild-type and glycomutant mammalian cells were effectively stratified using fluorescence signatures obtained from a single sensor element. Blinded unknowns generated from the tested cell types were identified with high accuracy (44 out of 48 samples), validating the robustness of the multichannel sensor. Notably, this selectivity-based high-throughput sensor differentiated between cells, employing a nondestructive protocol that required only a single well of a microplate for detection.

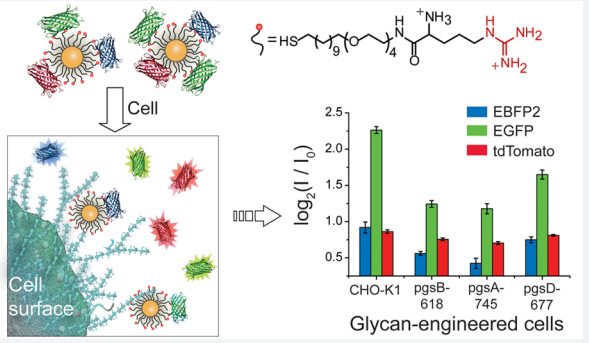

INTRODUCTION

Cell-surface glycans present an intricate and complex interface that plays a central role in numerous processes such as cell−cell recognition, pathogenesis, inflammation, cancer, and immune surveillance of tumors.[1,2] The composition of cell-surface glycans significantly varies with different cell states, such as stem-cell differentiation, tissue development, and cancer.[3,4] For example, sialyl Lewis X and sialyl Lewis A tetrasaccharides are overexpressed in certain cancers that are strongly metastatic.[5,6] These distinct cell-surface glycan "signatures" associated with each cell state provide key biomarkers for identifying healthy and malignant cell states with applications in both fundamental glycobiology and diagnostics.[7,8]

Profiling cell states based on glycosylation patterns is challenging due to the complex structures of the glycans, such as the presence of linkage isomers and branching events.[9] A number of strategies[10] including lectin arrays,[11] antiglycan antibodies,[12,13] and synthetic receptors[14−16] have been used to construct cell-surface saccharide biosensors. Application of these specificity-based sensors in identifying cell states is often limited owing to the difficulty in synthesis, poor stability of the constituents, high cost, and immunogenicity. Signature-based methods provide a potentially complementary alternative to specific biomarker identification: mass spectrometry of the cell-surface glycome has been employed successfully to differentiate between normal and cancerous cell states.[10,17,18] However, the added processing steps such as carbohydrate extraction, sophisticated analysis, and expensive instrumentation required by these methods restrict their use in rapid assays and introduce artifacts arising from the processing steps.

Direct readout of glycosylation signatures from the cell surfaces, particularly on living cells, would provide access to key glycomic information. Unbiased signature-based "chemical nose/tongue" methods that employ differential binding of analytes with sensor arrays provide a powerful alternative to biomarker-based approaches.[19] In this approach, a unique "fingerprint" is derived for each analyte interacting with the sensor, and subsequent comparison of the detected profile of a target analyte allows its classification and identification. Owing to the inherent generalizability of this strategy, signature-based sensing method presents a powerful tool for discriminating between different classes of analytes and their complex mixtures.[20,21] This sensing strategy has effectively been applied to detecting bioanalytes including proteins,[22−25] bacteria,[26,27] and mammalian cells,[28−31] even in biological matrices.[32,33] Despite the efficacy of array-based sensors in diagnostics, current systems are capable of producing only single channel measurements of the molecular recognition, requiring multiple spatially distinct sensor elements for identifying one analyte and limiting their application in rapid high-throughput screening of bioanalytes.[34]

Received: April 1, 2015
Published: June 8, 2015

DOI: 10.1021/acscentsci.5b00126
ACS Cent. Sci. 2015, 1, 191−197

In recent studies, we developed a supramolecular three-channel sensor system that uses different fluorescent proteins to generate a multiplex output.[35] Notably, the sensing approach utilizing simultaneous three-channel output requires only one sensor to correctly identify multiple cell types leading to detection from a *single* well of a microplate. We report here an important application of this strategy in differentiating mammalian cells based on their surface glycan signatures. We have fabricated a new three-channel sensor using gold nanoparticles featuring a glycan recognizing functional ligand[36−38] to successfully identify both glycomutant (mostly charged glycans) and glycosidase-modified wild-type cells. This identification was performed on living cells using the microplates they were grown on, demonstrating a non-destructive cell sensing method. Here, the directness of the measurement precludes additional processing steps such as extracting the glycans/proteoglycans or labeling the cells prior to analyses. The ability of this biosensor to detect cells based on overall glycan profiles, as opposed to the commonly used sensors focused on monosaccharides,[14] circumvents the limitations arising from the complexity of glycan structures and makes the sensor applicable to a vast number of cell types. Finally, this work provides fundamental insight into the molecular mechanism of previous studies on sensing mammalian cells that used selectivity-based array sensors,[28−31] revealing the direct connection between the cell-surface glycome and phenotypic differences of various cell types and states.

RESULTS AND DISCUSSION

We fabricated the three-channel sensor by noncovalent complexation of three fluorescent proteins (FPs) and arginine-ligand protected AuNP (**ArgNP**) (Figure 1A; see Figures S1−S7 for the synthesis and characterization of **ArgNP**). In this sensor, the FPs provide multivalent binding with the particles, as well as stable measurement of molecular recognition events between the particle and cell surfaces. We screened different fluorescent proteins and utilized an optimized set for fabricating the sensor: EBFP2 (blue), EGFP (green), and tdTomato (red). We selected this set of proteins based on the following criteria:[39] (a) the proteins bear net negative charges [calculated pK_a values of 6.4 (EBFP2), 6.0 (EGFP), and 6.5 (tdTomato) including His_6-tag] and show different binding affinities with the particle; (b) the FPs feature well-separated excitation and emission wavelengths with minimal spectral cross-talk, allowing us to obtain independent responses from each emission channel; (c) monomeric or tandem-dimeric structure of the FPs streamlines their use in displacement assays relative to other multimeric analogues; and (d) the photostability of the FPs provides reliable fluorescence outputs. For the recognition element, **ArgNP** with exposed arginine headgroup (Figure 1A) was used in the sensor based on the selective interaction of arginine with various glycans. For example, the arginine moiety is involved in high-affinity binding with the sulfonate groups of sulfated glycans (e.g., glycosaminoglycans)[36,37] as well as with carboxylate groups of hyaluronan and sialic acid through salt-bridge interactions, regulating the function of protein−glycan interface.[38]

Initially, we investigated the binding parameters of the **ArgNP**−FP complexes, since the binding thermodynamics of the particle and the FPs plays a central role in the sensor mechanism. Titration of a 1:1:1 mixture of the three FPs with **ArgNP** resulted in pronounced quenching of the FP

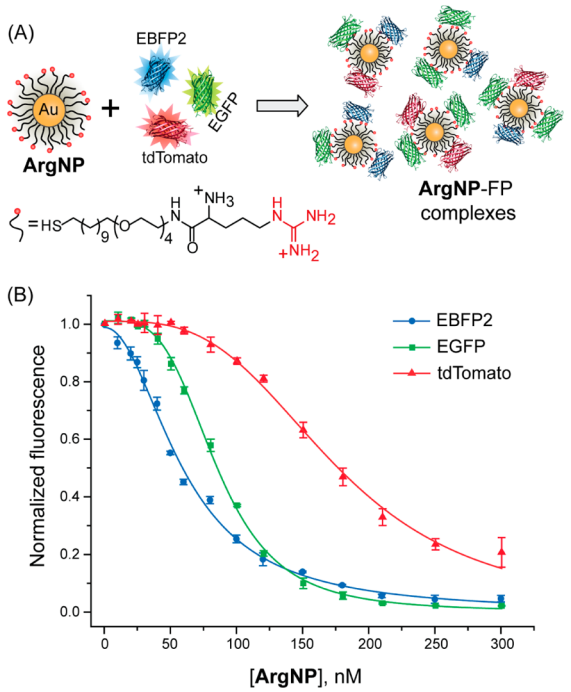

Figure 1. Assembly of the three-channel sensor. (A) Schematic illustration of the sensor fabrication by incubating the FPs and **ArgNP**. Structure of the ligand on the NP monolayer is shown at the bottom. (B) Fluorescence titration of an equimolar mixture of the three FPs by **ArgNP** in 5 mM sodium phosphate buffer (pH 7.4). The data points are obtained by averaging three replicates, and the error bars represent ±SD. The solid lines through the data represent the best nonlinear curve fitting.

fluorescence at NP surface saturation (Figure 1B), indicating that the FPs were quantitatively bound to the NP surface. Nonlinear least-squares curve fitting analysis of the fluorescence titration provided the dissociation constant (K_d) for each FP complex (Table S1), revealing high affinity of each FP for the particle. Despite the similarity in protein structures, the binding profiles of each protein varied significantly, suggesting that differential fluorescence responses would be generated for each FP upon interaction of the sensor with competing analytes such as mammalian cells.

The FP fluorescence is efficiently quenched by the particle core in the **ArgNP**−FP supramolecular complexes. When these complexes are incubated with cells, competitive binding of the particle to the cell results in rapid (seconds/minutes) displacement of FPs from the particle surface with consequent regeneration of FP fluorescence (Figure 2). The characteristic fluorescence signature enables us to discern between mammalian cells with different glycosylation patterns.

The utility of the sensor platform in rapid sensing of mammalian cells based on cell-surface glycosylation pattern was demonstrated first using glycomutant cells featuring different glycosaminoglycans (GAGs) as part of the cell surface proteoglycans. These isogenic cells (that possess the same genetic background) with differing cell surface glycomes provide a reliable testbed for discerning cell states based on characteristic glycosylation patterns.[40] We selected a set of GAG-mutated Chinese hamster ovary (CHO) cell types (CHO-K1, pgsB-618, pgsA-745, and pgsD-677)[41,42] as initial sensing targets. The role of cell surface glycan expression in cellular malignancies has been well established for the CHO cell

DOI: 10.1021/acscentsci.5b00126
ACS Cent. Sci. 2015, 1, 191−197

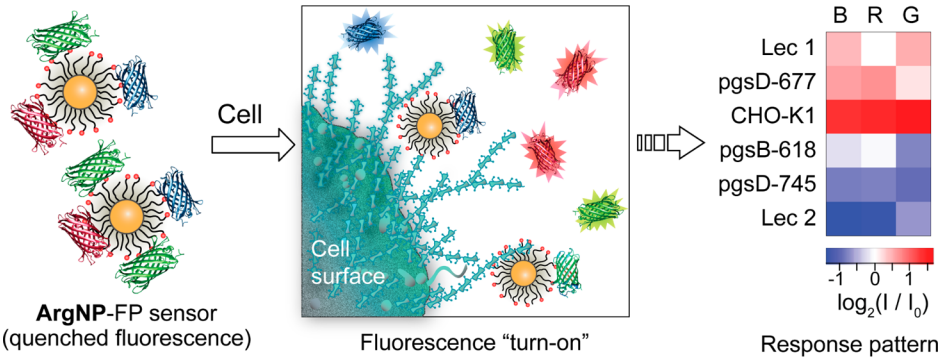

Figure 2. Schematic illustration of the principle of cell sensing using the multichannel approach. The heatplot is obtained by hierarchical clustering of the experimental data (average of 8 replicates) for all the glycomutated cells studied. The color codes of the heatplot represent the *z*-score of the fluorescence responses along each FP channel, where I and I_0 are the fluorescence with and without cells, respectively. B: EBFP2. R: tdTomato. G: EGFP.

Table 1. Characteristics of the CHO Cell Lines[41,43,44] Studied Using the Sensor Platform

cell line	biochemical defect	glycan composition	cell status
CHO-K1	none	wild-type	tumorigenic
pgsB-618	galactosyltransferase I deficient	proteoglycan deficient (15% of wild-type cells)	tumorigenic
pgsA-745	xylosyltransferase deficient	proteoglycan deficient (8% of wild-type cells)	nontumorigenic
pgsD-677	lacks *N*-acetylglucosaminyltransferase and glucuronyltransferase activities	HS deficient; produces 3−4-fold higher CS than CHO-K1 cells[a]	nontumorigenic
Lec-1	*N*-acetyl-D-glucosamine (GlcNAc) transferase I deficient	does not synthesize complex- or hybrid-type *N*-linked oligosaccharides	tumorigenic
Lec-2	unable to translocate CMP-sialic acid to Golgi apparatus	*N*- and *O*-linked sialic acid deficient	tumorigenic

[a]HS: heparan sulfate. CS: chondroitin sulfate.

types,[41,43] e.g., GAG-engineered CHO cell types that produce heparan sulfate (HS) proteoglycan <10% of the wild-type cells are tumorigenically transformed.[41] Different features of the CHO cell types related to our study and their states are presented in Table 1.

The first step of sensing was to "train" the sensor and build a statistical model for discerning the glycomic signatures of the respective cell lines. We determined that 10,000 cells provided reproducible fluorescence response based on single-well detection. Upon incubation of the sensor with the wild-type and GAG mutant cells cultured on a 96-well microplate, a characteristic fluorescence response pattern was generated corresponding to each cell type within minutes (Figure 3A). The fingerprint response patterns indicate differential interactions of the **ArgNP**−FP supramolecular complexes with the cell surfaces. The responses were compared across the cell types using an unsupervised agglomerative hierarchical clustering analysis (HCA) that classified the cells into separate branches of a cluster dendrogram (Figure 3B). Furthermore, the fluorescence responses were quantitatively analyzed using linear discriminant analysis (LDA), a statistical method that transforms multivariate data into a reduced number of variables through orthogonal linear combinations (see Supporting Information and ref 33 for details on the statistical method). LDA on the sensor outputs categorized them into four nonoverlapping clusters (Figure 3C) corresponding to each cell type, showing the ability of the sensor to rapidly distinguish between the GAG mutant cells.

To test the quality of the LDA classifier, leave-one-out cross-validation analysis was performed on all the response data. Jackknife analysis (see Supporting Information methods) on the training data set (4 cell lines × 8 replicates) revealed 100% between-group cross-validation accuracy (Figure 3D), indicating the LDA method to be a robust statistical tool for this system (see Table S2 for all the cells involved in this work). The Wilks lambda, a statistical parameter that represents the ratio between residual variance over the total variance, for the training set was derived to be 0.004 (F = 62.2, P = 0.0000), the small value of which supports LDA to be a strong model[45] for the present analyses.

Based on the fluorescence responses, the GAG mutant cells caused significantly less FP displacement from the particle surface than the wild-type CHO cells. This result is anticipated, as the lesser amount of negatively charged GAGs on these mutant cell surfaces should result in lesser FP displacement based on electrostatic interactions. Interestingly, pgsD-677 cells lacking HS, the most sulfated glycan, produced higher regenerated fluorescence compared to the other two GAG mutant cells containing low level of cell-surface HS. Presumably, the higher fluorescence response from the HS-deficient pgsD-677 cells originates from the preferential interactions of **ArgNP** with chondroitin sulfate (CS) along with other glycans present on the cell surface. In fact, the GAG pool of wild-type CHO cell surfaces has been shown to consist of about 70% HS and 30% CS.[41] The variation in fluorescence responses as a function of small changes on cell surface GAGs demonstrates the ability of the sensor to detect subtle change in glycosylation.

There is the possibility of dissimilar downstream processes of the mutated cell lines: in addition to glycans the cell surfaces may differ in other surface biomolecules such as proteins and lipids that could interact with the cationic particle. We compared sensor responses from the GAG-mutated cell lines with that of glycosidic enzyme-treated wild-type cells (diminished glycans) to demonstrate the glycan basis of our sensor system. In these studies, wild-type CHO-K1 cells were

DOI: 10.1021/acscentsci.5b00126
ACS Cent. Sci. 2015, 1, 191−197

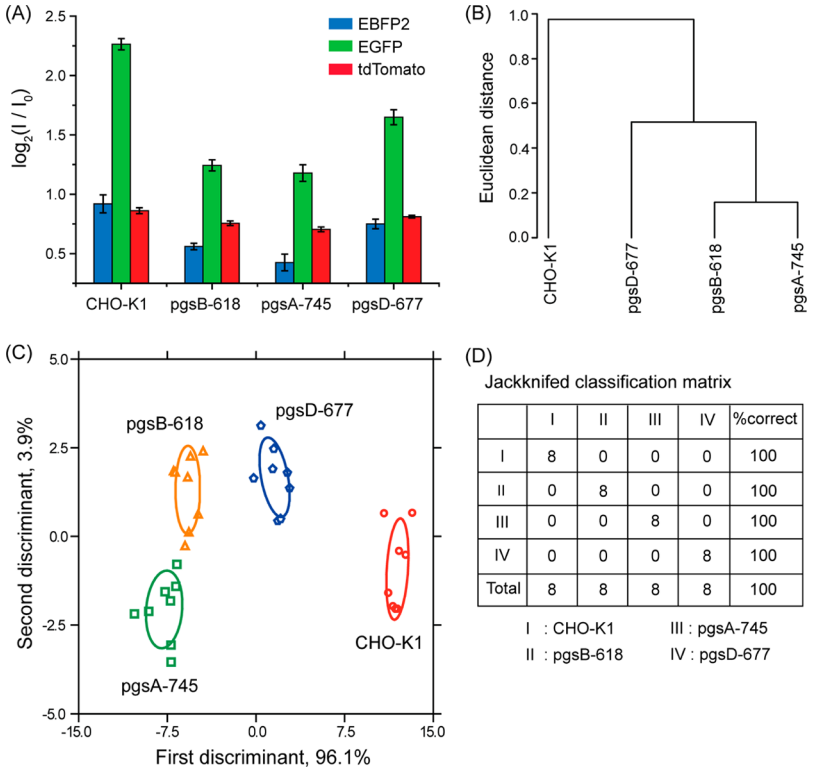

	I	II	III	IV	%correct
I	8	0	0	0	100
II	0	8	0	0	100
III	0	0	8	0	100
IV	0	0	0	8	100
Total	8	8	8	8	100

Figure 3. Fluorescence fingerprints of GAG-engineered cells. (A) Fluorescence responses of the cells upon incubation with the sensor for 30 min, where I_0 and I are respectively the fluorescence before and after the addition of the sensor to the cells. The data are obtained by averaging eight independent replicates, and the error bars represent the ±SD. (B) The dendrogram derived from unsupervised hierarchical clustering analysis of the fluorescence responses that are averages of 8 replicates. HCA was performed using the average linkage method, where the distance metric is Euclidean distance. (C) LDA score plot of the fluorescence responses. The analysis resulted in canonical scores with three discriminants explaining 96.1 and 3.9% of total variance and was plotted with 95% confidence ellipses around the centroid of each group. (D) Cross-validation of LDA on the data set. Jackknife analysis using leave-one-out exercise was performed on all the replicate data.

Table 2. Glycosidic Enzymes Used To Cleave Cell Surface Glycans from CHO Cells, Their Functions, and the Expected Similarity to the GAG-Engineered Cell Lines

enzyme	function	expected similarity with
heparinase I and III	cleaves heparin and heparan sulfate at the 1−4 linkages between hexosamines and O-sulfated iduronic acids, yielding mainly disaccharides	HS-deficient cell type (e.g., pgsD-677)
chondroitinase ABC	cleaves chondroitin 4-sulfate, chondroitin 6-sulfate, and dermatan sulfate, and acts slowly on hyaluronate	CS-deficient cell type
heparinase + chondroitinase ABC	combined effect of heparinase I and chondroitinase ABC, cleaving major GAGs	HS- and CS-deficient cell type (possibly pgsB-618, pgsA-745)
crude *F. heparinum* enzymes	contains chondroitinase, dermatanase, heparinase, and heparitinase activity[46] and thus degrades all the sulfated GAGs	GAG-deficient cell type (e.g., pgsB-618 and pgsA-745)

treated with the glycosidic enzymes (Table 2) at a concentration that resulted in maximum GAG cleavage. We monitored the cleavage by an increase in absorbance at 232 nm, owing to an unsaturated double bond introduced during the cleavage between hexosamines and uronic acids.[47] Upon incubation of the sensor with the enzyme-treated cells, good similarity in fluorescence response was observed between the enzyme-treated and glycomutant cell lines (Figure 4A). We performed unsupervised HCA to visualize the relation between the enzyme-treated and the glycomutated cells. As shown in Figure 4B, the pgsD-677 cells and heparinase-treated cells were clustered together, indicating the similarity of HS-cleaved and HS-deficient cells. Likewise, pgsB-618 and pgsA-745 cells were grouped with chondroitinase and (chondroitinase + heparinase)-treated cells, with close proximity to crude *Flavobacterium heparinum* enzyme-treated cells. While the absolute values were somewhat different, the general trend of the enzyme-treated cells was quite similar to that of the GAG-mutated cells. Taken together, we can confidently conclude that NP−GAG interactions are the major contributor in generating the sensor responses.

An important outcome from the enzymatic GAG-degradation study is the contribution of CS to the fluorescence responses. The higher fluorescence response from HS-deficient pgsD-677 cell line indicates a temporal structure of GAGs in the glycocalyx of the wild-type CHO cells, where CS can be exposed after heparinase I treatment. In fact, the sensor response is considerably diminished following chondroitinase treatment, reflecting a higher affinity of the particles to CS. Therefore, the molecular recognition of **ArgNP** and different glycans is quite selective, making the sensor applicable to diverse cell types and states.

Our sensor system could reliably differentiate between cells featuring changes in negatively charged GAG-modified cells.

DOI: 10.1021/acscentsci.5b00126
ACS Cent. Sci. 2015, 1, 191−197

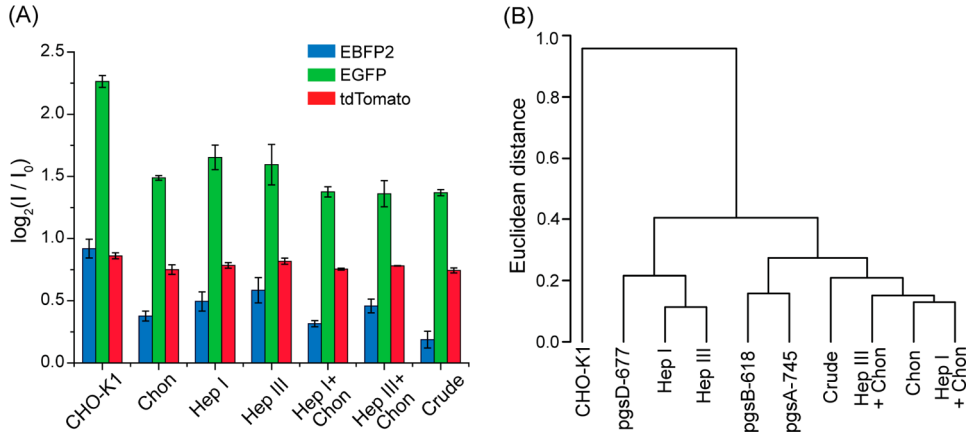

Figure 4. Comparison between fluorescence signatures of glycoengineered and glycosidic enzyme-treated CHO cells. (A) Fluorescence responses along the three FP channels upon interaction with the wild-type and glycosidic enzyme-treated CHO cells, where I_0 and I are respectively the fluorescence before and after the addition of the sensor to the cells. The data are obtained by averaging five replicates and the error bars represent the ±SD. (B) The cluster dendrogram obtained from HCA on the average fluorescence responses. HCA was performed using the average linkage method, where the distance metric is Euclidean distance. Chon: chondroitinase ABC. Hep I: heparinase I. Hep III: heparinase III. Crude: crude enzyme mixture isolated from *F. heparinum* cells.

Distinguishing cells with more subtle variations in their cell surface glycome poses a challenging task. To assess the broader applicability of the sensor to other glycosylation changes, we used two mutated CHO cell lines as a testbed (Table 1): (i) Lec-1 cells,[44] with *N*-acetyl-D-glucosamine transferase I deficiency lacking complex and hybrid type *N*-glycans, resulting in increase of high-mannose type *N*-glycans instead; (ii) Lec-2 cells,[48] with a mutation in the gene encoding a sialyltransferase—the transporter of CMP-sialic acid from the cytosol to Golgi vesicle—resulting in dramatically reduced sialic acid in their glycocalyx. The fluorescence responses from Lec-1 and Lec-2 cells were quantitatively different from each other as well as from the parental CHO-K1 cells (Figure 5A). LDA of the fluorescence responses clustered the three cells into three distinct groups (Figure 5B), demonstrating their effective classification. While noncharged glycan-engineered cells were efficiently distinguished, the sensor was further tested on cell types with distinct phenotypes, featuring wild-type glycomic signatures. Isogenic murine mammary cell lines possessing normal, cancerous, and metastatic phenotypes (CDβGeo, pTD, and V14, respectively) generated characteristic fluorescence responses that grouped the cells into three distinct clusters (Figure S8), validating the versatility of the sensor.

After demonstrating the ability of our system to differentiate between both glycomutants and glycosidase-modified cells, we assessed the contribution from each FP in generating the differential fluorescence responses. Analysis of the fluorescence responses from the six cell lines revealed that each of the FP channels significantly impacts the overall sensing capabilities (see discussion in the Supporting Information, and Figures S9, S10, and S11). In addition, correlation (Pearson's) of the canonical scores along each discriminant with the fluorescence response from the FPs showed the contribution from each FP (Figure S10), reflecting the involvement of all the FPs in the fluorescence displacement process.

The goal of our study was to identify cells based on their surface glycome. The clustering studies described above are the first step in generating the sensor system, in effect training the system to identify glycomic signatures. Identification of unknowns demonstrates both the robustness of our clustering strategy and the potential utility of this method for diagnostic

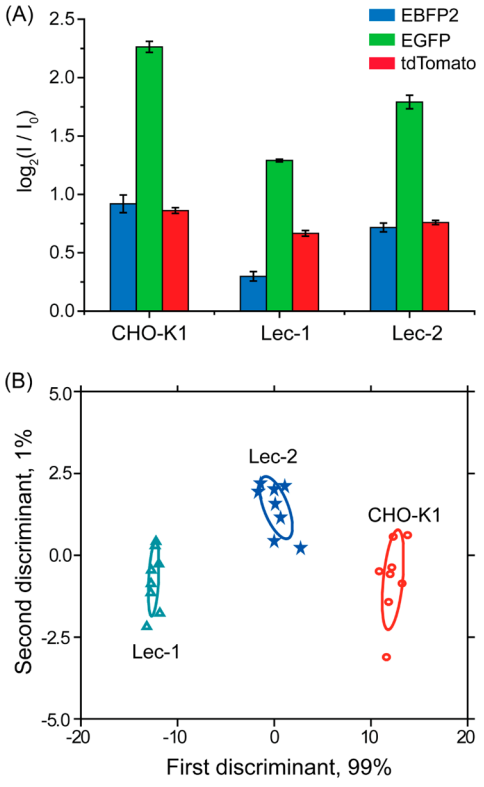

Figure 5. Differentiation of CHO cell types with *N*-linked carbohydrate and sialic acid deficiency. (A) Fluorescence responses along the three FP channels upon interaction with the parental and the Lec cells, where I_0 and I are respectively the fluorescence before and after the addition of the sensor to the cells. The data are obtained by averaging eight replicates, and the error bars represent the ±SD. (B) LDA of the fluorescence responses resulted in canonical scores with two discriminants explaining 99.0 and 1.0% of total variance and were plotted with 95% confidence ellipses around the centroid of each group.

applications. We utilized the six CHO cell lines as the training set and performed tests on a randomized set of 48 unknown samples prepared from these cells that were blinded to the researcher running the test and the analyses. Identification was

DOI: 10.1021/acscentsci.5b00126
ACS Cent. Sci. 2015, 1, 191−197

done using the Mahalanobis distance-square[49] (defined as the distance between a point and a distribution) proximities of the unknowns to the centroid of each group, established from the training set (see Supporting Information methods). The test was able to identify 44 samples correctly (92%, Table S6), demonstrating the reproducibility of the responses and reliability of the sensor in detecting cells. Notably, the efficacy of our approach to identify isogenic mammalian cells bearing different negatively charged glycan composition (GAG, hyaluronic acid, sialylated glycans) indicates the differential specificities of sensor toward the cell-surface glycans. Given the efficiency of the electrostatic interaction-based sensors in identifying different cell types/states,[28−31,35,50,51] the present three-channel sensor should enable screening of a far larger variety of cells, complementing existing glycan-based cell detection strategies.

CONCLUSIONS

In summary, we have developed a rapid and efficient multichannel sensor that employs supramolecular interactions of fluorescent proteins and a functionalized gold NP. This system responds to different glycan patterns, both charged and noncharged, on cell surfaces. Healthy and cancerous cells with the same genetic background and exhibiting different cell surface glycome signatures were effectively discerned within a single well of a microplate without extracting proteoglycans or labeling specific sugar units. Significantly, the present study demonstrated the role of glycans in identifying cell states using nonspecific sensors, an important step forward to designing effective signature-based biodiagnostics. Taken together, the ability to recognize cells combined with the high-throughput features of the sensor holds great promise in personalized screening of disease states, and cell-based profiling of the mechanisms of carbohydrate therapeutics.[52] In addition, the selectivity of the nanoparticle−glycan interactions opens up new opportunities for developing inhibitors for physiological protein−glycan binding,[53] point-of-care assays for glycan biomarkers in biofluids,[54] and targeted imaging agents.[1,15]

ASSOCIATED CONTENT

Supporting Information

The following file is available free of charge on the ACS Publications website at DOI: 10.1021/acscentsci.5b00126.

Experimental details, characterization data, statistical analyses, discussion of FPs, and fluorescence data (PDF)

AUTHOR INFORMATION

Corresponding Author

*E-mail: rotello@chem.umass.edu.

Author Contributions

§N.D.B.L., R.M., and B.D. contributed equally to the work.

Notes

The authors declare no competing financial interest.

ACKNOWLEDGMENTS

This work was supported by the NIH (GM0771730).

REFERENCES

(1) Dube, D. H.; Bertozzi, C. R. Glycans in cancer and inflammation. Potential for therapeutics and diagnostics. *Nat. Rev. Drug Discovery* **2005**, *4*, 477−488.

(2) Varki, A.; Kannagi, R.; Toole, B. P. Glycosylation changes in cancer. In *Essentials of Glycobiology*, 2nd ed.; Varki, A., et al., Eds.; Cold Spring Harbor Laboratory Press: New York, 2009.

(3) Lanctot, P. M.; Gage, F. H.; Varki, A. P. The glycans of stem cells. *Curr. Opin. Chem. Biol.* **2007**, *11*, 373−380.

(4) Hakomori, S. Glycosylation defining cancer malignancy: New wine in an old bottle. *Proc. Natl. Acad. Sci. U.S.A.* **2002**, *99*, 10231−10233.

(5) Engelstaedter, V.; Fluegel, B.; Kunze, S.; Mayr, D.; Friese, K.; Jeschke, U.; Bergauer, F. Expression of the carbohydrate tumour marker Sialyl Lewis A, Sialyl Lewis X, Lewis Y and Thomsen-Friedenreich antigen in normal squamous epithelium of the uterine cervix, cervical dysplasia and cervical cancer. *Histol. Histopathol.* **2012**, *27*, 507−514.

(6) Kirmiz, C.; Li, B. S.; An, H. J.; Clowers, B. H.; Chew, H. K.; Lam, K. S.; Ferrige, A.; Alecio, R.; Borowsky, A. D.; Sulaimon, S.; Lebrilla, C. B.; Miyamoto, S. A serum glycomics approach to breast cancer biomarkers. *Mol. Cell. Proteomics* **2007**, *6*, 43−55.

(7) Lebrilla, C. B.; An, H. J. The prospects of glycan biomarkers for the diagnosis of diseases. *Mol. BioSyst.* **2009**, *5*, 17−20.

(8) Kim, Y. J.; Varki, A. Perspectives on the significance of altered glycosylation of glycoproteins in cancer. *Glycoconjugate J.* **1997**, *14*, 569−576.

(9) Jelinek, R.; Kolusheva, S. Carbohydrate biosensors. *Chem. Rev.* **2004**, *104*, 5987−6015.

(10) Vanderschaeghe, D.; Festjens, N.; Delanghe, J.; Callewaert, N. Glycome profiling using modern glycomics technology: Technical aspects and applications. *Biol. Chem.* **2010**, *391*, 149−161.

(11) Hirabayashi, J.; Yamada, M.; Kuno, A.; Tateno, H. Lectin microarrays: Concept, principle and applications. *Chem. Soc. Rev.* **2013**, *42*, 4443−4458.

(12) Dexlin, L.; Ingvarsson, J.; Frendeus, B.; Borrebaeck, C. A. K.; Wingren, C. Design of recombinant antibody microarrays for cell surface membrane proteomics. *J. Proteome Res.* **2008**, *7*, 319−327.

(13) Cunningham, S.; Gerlach, J. Q.; Kane, M.; Joshi, L. Glyco-biosensors: Recent advances and applications for the detection of free and bound carbohydrates. *Analyst* **2010**, *135*, 2471−2480.

(14) Arnaud, J.; Audfray, A.; Imberty, A. Binding sugars: From natural lectins to synthetic receptors and engineered neolectins. *Chem. Soc. Rev.* **2013**, *42*, 4798−4813.

(15) Xu, X. D.; Cheng, H.; Chen, W. H.; Cheng, S. X.; Zhuo, R. X.; Zhang, X. Z. In situ recognition of cell-surface glycans and targeted imaging of cancer cells. *Sci. Rep.* **2013**, *3*, 2679.

(16) Bicker, K. L.; Sun, J.; Harrell, M.; Zhang, Y.; Pena, M. M.; Thompson, P. R.; Lavigne, J. J. Synthetic lectin arrays for the detection and discrimination of cancer associated glycans and cell lines. *Chem. Sci.* **2012**, *3*, 1147−1156.

(17) Sethi, M. K.; Thaysen-Andersen, M.; Smith, J. T.; Baker, M. S.; Packer, N. H.; Hancock, W. S.; Fanayan, S. Comparative N-glycan profiling of colorectal cancer cell lines reveals unique bisecting GlcNAc and α-2,3-linked sialic acid determinants are associated with membrane proteins of the more metastatic/aggressive cell lines. *J. Proteome Res.* **2014**, *13*, 277−288.

(18) Yang, S.; Eshghi, S. T.; Chiu, H. C.; DeVoe, D. L.; Zhang, H. Glycomic analysis by glycoprotein immobilization for glycan extraction and liquid chromatography on microfluidic chip. *Anal. Chem.* **2013**, *85*, 10117−10125.

(19) Albert, K. J.; Lewis, N. S.; Schauer, C. L.; Sotzing, G. A.; Stitzel, S. E.; Vaid, T. P.; Walt, D. R. Cross-reactive chemical sensor arrays. *Chem. Rev.* **2000**, *100*, 2595−2626.

(20) Greene, N. T.; Shimizu, K. D. Colorimetric molecularly imprinted polymer sensor array using dye displacement. *J. Am. Chem. Soc.* **2005**, *127*, 5695−5700.

(21) Wright, A. T.; Anslyn, E. V. Differential receptor arrays and assays for solution-based molecular recognition. *Chem. Soc. Rev.* **2006**, *35*, 14−28.

(22) You, C. C.; Miranda, O. R.; Gider, B.; Ghosh, P. S.; Kim, I. B.; Erdogan, B.; Krovi, S. A.; Bunz, U. H. F.; Rotello, V. M. *Nat. Nanotechnol.* **2007**, *2*, 318.

DOI: 10.1021/acscentsci.5b00126
ACS Cent. Sci. 2015, 1, 191−197

(23) Margulies, D.; Hamilton, A. D. Protein recognition by an ensemble of fluorescent DNA G-quadruplexes. *Angew. Chem., Int. Ed.* **2009**, *48*, 1771−1774.
(24) Wright, A. T.; Griffin, M. J.; Zhong, Z. L.; McCleskey, S. C.; Anslyn, E. V.; McDevitt, J. T. Differential receptors create patterns that distinguish various proteins. *Angew. Chem., Int. Ed.* **2005**, *44*, 6375−6378.
(25) Moyano, D. F.; Rana, S.; Bunz, U. H. F.; Rotello, V. M. Gold nanoparticle-polymer/biopolymer complexes for protein sensing. *Faraday Discuss.* **2011**, *152*, 33−42.
(26) Phillips, R. L.; Miranda, O. R.; You, C. C.; Rotello, V. M.; Bunz, U. H. F. Rapid and efficient identification of bacteria using gold-nanoparticle - poly(para-phenyleneethynylene) constructs. *Angew. Chem., Int. Ed.* **2008**, *47*, 2590−2594.
(27) Duarte, A.; Chworos, A.; Flagan, S. F.; Hanrahan, G.; Bazan, G. C. Identification of bacteria by conjugated oligoelectrolyte/single-stranded DNA electrostatic complexes. *J. Am. Chem. Soc.* **2010**, *132*, 12562−12564.
(28) Bajaj, A.; Miranda, O. R.; Kim, I. B.; Phillips, R. L.; Jerry, D. J.; Bunz, U. H. F.; Rotello, V. M. Detection and differentiation of normal, cancerous, and metastatic cells using nanoparticle-polymer sensor arrays. *Proc. Natl. Acad. Sci. U.S.A.* **2009**, *106*, 10912−10916.
(29) El-Boubbou, K.; Zhu, D. C.; Vasileiou, C.; Borhan, B.; Prosperi, D.; Li, W.; Huang, X. F. Magnetic glyco-nanoparticles: A tool to detect, differentiate, and unlock the glyco-codes of cancer via magnetic resonance imaging. *J. Am. Chem. Soc.* **2010**, *132*, 4490−4499.
(30) Bajaj, A.; Rana, S.; Miranda, O. R.; Yawe, J. C.; Jerry, D. J.; Bunz, U. H. F.; Rotello, V. M. Cell surface-based differentiation of cell types and cancer states using a gold nanoparticle-GFP based sensing array. *Chem. Sci.* **2010**, *1*, 134−138.
(31) Scott, M. D.; Dutta, R.; Haldar, M. K.; Guo, B.; Friesner, D. L.; Mallik, S. Differentiation of prostate cancer cells using flexible fluorescent polymers. *Anal. Chem.* **2012**, *84*, 17−20.
(32) De, M.; Rana, S.; Akpinar, H.; Miranda, O. R.; Arvizo, R. R.; Bunz, U. H. F.; Rotello, V. M. Sensing of proteins in human serum using conjugates of nanoparticles and green fluorescent protein. *Nat. Chem.* **2009**, *1*, 461−465.
(33) Rana, S.; Singla, A. K.; Bajaj, A.; Elci, S. G.; Miranda, O. R.; Mout, R.; Yan, B.; Jirik, F. R.; Rotello, V. M. Array-based sensing of metastatic cells and tissues using nanoparticle-fluorescent protein conjugates. *ACS Nano* **2012**, *6*, 8233−8240.
(34) Potyrailo, R. A.; Mirsky, V. M. Combinatorial and high-throughput development of sensing materials: The first 10 years. *Chem. Rev.* **2008**, *108*, 770−813.
(35) Rana, S.; Le, N. D. B.; Mout, R.; Saha, K.; Tonga, G. Y.; Bain, R. E. S.; Miranda, O. R.; Rotello, C. M.; Rotello, V. M. A multichannel nanosensor for instantaneous readout of cancer drug mechanisms. *Nat. Nanotechnol.* **2015**, *10*, 65−69.
(36) Hileman, R. E.; Fromm, J. R.; Weiler, J. M.; Linhardt, R. J. Glycosaminoglycan-protein interactions: Definition of consensus sites in glycosaminoglycan binding proteins. *BioEssays* **1998**, *20*, 156−167.
(37) Fromm, J. R.; Hileman, R. E.; Caldwell, E. E. O.; Weiler, J. M.; Linhardt, R. J. Differences in the interaction of heparin with arginine and lysine and the importance of these basic amino acids in the binding of heparin to acidic fibroblast growth factor. *Arch. Biochem. Biophys.* **1995**, *323*, 279−287.
(38) Faller, C. E.; Guvench, O. Terminal sialic acids on CD44 N-glycans can block hyaluronan binding by forming competing intramolecular contacts with arginine sidechains. *Proteins* **2014**, *82*, 3079−3089.
(39) Shaner, N. C.; Steinbach, P. A.; Tsien, R. Y. A guide to choosing fluorescent proteins. *Nat. Methods* **2005**, *2*, 905−909.
(40) Sasisekharan, R.; Shriver, Z.; Venkataraman, G.; Narayanasami, U. Roles of heparan-sulphate glycosaminoglycans in cancer. *Nat. Rev. Cancer* **2002**, *2*, 521−528.
(41) Esko, J. D.; Rostand, K. S.; Weinke, J. L. Tumor-formation dependent on proteoglycan biosynthesis. *Science* **1988**, *241*, 1092−1096.
(42) Esko, J. D.; Weinke, J. L.; Taylor, W. H.; Ekborg, G.; Roden, L.; Anantharamaiah, G.; Gawish, A. Inhibition of chondroitin and heparan-sulfate biosynthesis in chinese-hamster ovary cell mutants defective in Galactosyltransferase-I. *J. Biol. Chem.* **1987**, *262*, 12189−12195.
(43) Ripka, J.; Shin, S. I.; Stanley, P. Decreased tumorigenicity correlates with expression of altered cell-surface carbohydrates in Lec9 CHO cells. *Mol. Cell. Biol.* **1986**, *6*, 1268−1275.
(44) Stanley, P.; Caillibot, V.; Siminovitch, L. Selection and characterization of 8 phenotypically distinct lines of lectin-resistant chinese-hamster ovary cells. *Cell* **1975**, *6*, 121−128.
(45) Rencher, A. C. *Methods of multivariate analysis*, 1st ed.; John Wiley & Sons: New York, 1995; p 180.
(46) Korn, E. D. Inactivation of lipoprotein lipase by heparinase. *J. Biol. Chem.* **1957**, *226*, 827−832.
(47) Linker, A.; Hovingh, P. The enzymatic degradation of heparin and heparitin sulfate I. The fractionation of a crude heparinase from flavobacteria. *J. Biol. Chem.* **1965**, *240*, 3724−3728.
(48) Deutscher, S. L.; Nuwayhid, N.; Stanley, P.; Briles, E. I. B.; Hirschberg, C. B. Translocation across golgi vesicle membranes - a CHO glycosylation mutant deficient in CMP-sialic acid transport. *Cell* **1984**, *39*, 295−299.
(49) Mahalanobis, P. C. On the generalised distance in statistics. *Proc. Natl. Inst. Sci. India* **1936**, *2*, 49−55.
(50) Peng, G.; Tisch, U.; Adams, O.; Hakim, M.; Shehada, N.; Broza, Y. Y.; Billan, S.; Abdah-Bortnyak, R.; Kuten, A.; Haick, H. Diagnosing lung cancer in exhaled breath using gold nanoparticles. *Nat. Nanotechnol.* **2009**, *4*, 669−673.
(51) Kong, H.; Liu, D.; Zhang, S. C.; Zhang, X. R. Protein sensing and cell discrimination using a sensor array based on nanomaterial-assisted chemiluminescence. *Anal. Chem.* **2011**, *83*, 1867−1870.
(52) Ernst, B.; Magnani, J. L. From carbohydrate leads to glycomimetic drugs. *Nat. Rev. Drug Discovery* **2009**, *8*, 661−677.
(53) van Kooyk, Y.; Rabinovich, G. A. Protein-glycan interactions in the control of innate and adaptive immune responses. *Nat. Immunol.* **2008**, *9*, 593−601.
(54) Ruhaak, L. R.; Miyamoto, S.; Lebrilla, C. B. Developments in the identification of glycan biomarkers for the detection of cancer. *Mol. Cell. Proteomics* **2013**, *12*, 846−855.

DOI: 10.1021/acscentsci.5b00126
ACS Cent. Sci. 2015, 1, 191−197